agronomy

MDPI

Article

Use of Sentinel-2 Derived Vegetation Indices for Estimating fPAR in Olive Groves

Luisa Leolini [1], Marco Moriondo [2,*], Riccardo Rossi [1], Edoardo Bellini [1], Lorenzo Brilli [2], Álvaro López-Bernal [3], Joao A. Santos [4], Helder Fraga [4], Marco Bindi [1], Camilla Dibari [1] and Sergi Costafreda-Aumedes [1,2]

[1] Department of Agriculture, Food, Environment and Forestry (DAGRI), University of Florence, Piazzale delle Cascine 18, 50144 Florence, Italy; luisa.leolini@unifi.it (L.L.); r.rossi@unifi.it (R.R.); edoardo.bellini@unifi.it (E.B.); marco.bindi@unifi.it (M.B.); camilla.dibari@unifi.it (C.D.); sergi.costafreda@ibe.cnr.it (S.C.-A.)
[2] National Research Council of Italy, Institute of BioEconomy (CNR-IBE), Via G. Caproni 8, 50145 Florence, Italy; lorenzo.brilli@ibe.cnr.it
[3] Department of Agronomy, Campus de Rabanales, University of Cordoba, Edificio C4, 14071 Cordoba, Spain; g42lobea@uco.es
[4] Centre for the Research and Technology of Agro-Environmental and Biological Sciences (CITAB), Universidade de Trás-os-Montes e Alto Douro (UTAD), 5000-801 Vila Real, Portugal; jsantos@utad.pt (J.A.S.); hfraga@utad.pt (H.F.)
* Correspondence: marco.moriondo@cnr.it

Abstract: Olive tree cultivation is currently a dominant agriculture activity in the Mediterranean basin, where the increasing impact of climate change coupled with the inefficient management of olive groves is negatively affecting olive oil production and quality in some marginal areas. In this context, satellite imagery may help to monitor crop growth under different environmental conditions, thus providing useful information for optimizing olive grove management and final production. However, the spatial resolution of freely-available satellite products is not yet adequate to estimate plant biophysical parameters in complex agroecosystems such as olive groves, where both olive trees and grass cover contribute to the vegetation indices (VIs) signal at pixel scale. The aim of this study is therefore to test a disentangling procedure to partition the VIs signal among the different components of the agroecosystem to use this information for the monitoring of olive growth processes during the season. Specifically, five VIs (GEMI, MCARI2, NDVI, OSAVI, MCARI2/OSAVI) as recorded by Sentinel-2 at a spatial resolution of 10 m over five olive groves in the Montalbano area (Tuscany, Central Italy), were tested as a proxy for olive tree intercepted radiation. The olive tree volume per pixel was initially used to linearly rescale the VIs signal into the relevant value for the grass cover and olive trees. The models, describing the relationship between rescaled VIs and observed fraction of Photosynthetically Active Radiation (fPAR), were fitted and then validated against independent datasets. While in the calibration phase, a greater robustness at predicting fPAR was obtained using NDVI (r = 0.96 and $RRMSE$ = 9.86), the validation results demonstrating that GEMI and MCARI2/OSAVI provided the highest performances (GEMI: r = 0.89 and $RRMSE$ = 21.71; MCARI2/OSAVI: r = 0.87 and $RRMSE$ = 25.50), in contrast to MCARI2 that provided the lowest (r = 0.67 and $RRMSE$ = 36.78). These results may be related to the VIs' intrinsic features (e.g., lower sensitivity to atmosphere and background effects), which make some of these indices, compared to others, less sensitive to saturation effects by improving fPAR estimation (e.g., GEMI vs. NDVI). On this basis, this study evidenced the need to improve the current methodologies to reduce inter-row effects and select appropriate VIs for fPAR estimation, especially in complex agroecosystems where inter-row grass growth may affect remote sensed-derived VIs signal at an inadequate pixel resolution.

Keywords: fpar; olive trees; remote sensing; satellite imagery; monitoring

Citation: Leolini, L.; Moriondo, M.; Rossi, R.; Bellini, E.; Brilli, L.; López-Bernal, Á.; Santos, J.A.; Fraga, H.; Bindi, M.; Dibari, C.; et al. Use of Sentinel-2 Derived Vegetation Indices for Estimating fPAR in Olive Groves. *Agronomy* **2022**, *12*, 1540. https://doi.org/10.3390/agronomy12071540

Academic Editor: Dimitrios D. Alexakis

Received: 24 May 2022
Accepted: 23 June 2022
Published: 27 June 2022

Publisher's Note: MDPI stays neutral with regard to jurisdictional claims in published maps and institutional affiliations.

1. Introduction

Olive tree cultivation is one of the most important agricultural systems in Italy, extending over more than 1 million ha and mainly concentrated in the southern and central regions [1]. Despite its economic and environmental relevance, this cultivation is currently threatened by climate change [2–5] and hampered by the lack of modern agronomic management strategies, favoring the progressive abandonment of olive groves [6,7]. By contrast, the recovery of this cultivation over abandoned areas and an increase in the productive potential of marginal olive groves could enhance farmers' income and contribute to preserving and maintaining the rural landscape (CATChCO2-live project, 2017).

In order to address this solution, remote sensing technologies may help farmers to adopt specific management practices that increase olive production and reduce waste and input requirements [8,9]. When applied in olive tree cultivations, remote sensing technologies can provide information about the olive tree biophysical and dimensional properties such as chlorophyll content [10], soil and plant water status [11], vegetation growth and canopy dimensions [12], pest and disease outbreaks [13], and management impacts [14]. The olive grove monitoring is performed by correlating the Vegetation Indices (VIs) from high-resolution images with variables such as Leaf Area Index (LAI), fraction of Photosynthetically Active Radiation (fPAR), soil water dynamics, Net Ecosystems Exchange (NEE), etc. [15–17]. In particular, fPAR, representing the amount of solar radiation intercepted by leaves and used for the photosynthesis process, can be coupled with evapotranspiration estimates to simulate olive grove primary production [18]. In this regard, the multi-temporal monitoring of fPAR with remote sensing technologies may allow for assessing the seasonal trend of biomass accumulation and abiotic stresses affecting the final production in olive groves.

The most used VI for deriving fPAR and ensuring ecosystem monitoring is the Normalized Difference Vegetation Index (NDVI). However, given well-known issues related to its saturation and sensitivity to atmospheric and background effects [19,20], alternative VIs were frequently developed and adopted to accurately estimate plant biophysical properties under different environmental conditions. Among these, the GEMI index [21], developed to reduce the effect of the atmosphere, the OSAVI index [22], to reduce the effect of soil background on sparse and dry vegetation, the MCARI2 [23] to improve the predictions of some plant biophysical parameters (e.g., LAI), and MCARI/OSAVI and TCARI/OSAVI, which have been found to be useful solutions to further minimize the errors derived from soil background effects and vegetative parameters (e.g., LAI) variability [10,24], are promising VIs to avoid NDVI-use constraints.

However, with olive trees the current spatial resolution of the Copernicus satellite products does not allow one to accurately disentangle the tree component from the grass layer. Thus, the adoption of segmentation algorithms and appropriated methodologies become essential to separate the VIs contribution between the woody (i.e., olive trees) and grass layers [18]. Although high spatial resolution (~3 cm) of sensors installed on an Unmanned Aerial Vehicle (UAV) can overcome these issues, UAV technology often requires high costs due to equipment and field campaigns [25]. The use of multi-temporal data acquired from satellite freely accessible web platforms (https://scihub.copernicus.eu; accessed on 12 January 2022), can provide a suitable alternative to reduce these costs. For this reason, the development of low-cost methodologies able to rescale VIs contribution of satellite images and to disentangle grass cover from olive tree canopies is increasingly needed.

Building on these premises, this study aims at testing a methodology for partitioning the contribution of olive trees to VIs in Sentinel-2 imageries, to be used as a proxy for improving the fPAR estimation and monitoring at sub-field level during the growing season. The proposed methodology was calibrated and validated in five olive groves located in the Montalbano area (Tuscany, Central Italy), which encompasses different climates, plant density, pruning system and soil management practices and considers the performances of different VIs, namely GEMI, MCARI2, NDVI, OSAVI and MCARI2/OSAVI at

the pixel resolution of 10 m under different years. The results are discussed highlighting the potential contribution of this approach to optimize the farm schedule and aid farmers' decision making, by also suggesting possible implications in crop modeling for improving the within-field olive tree monitoring and for assessing the climate change impacts on olive groves.

2. Materials and Methods

2.1. Study Area

The study area is located in the Montalbano district (Lat. 43.81°, Long. 10.97°), Tuscany Region (Italy; Figure 1). The area has a Mediterranean climate, with mild winters, hot and dry summers and precipitation mainly concentrated in spring and autumn. Mean annual air temperature is 14.5 °C (1950–2020 average), with the average maximum and minimum recorded in July (30.1 °C) and January (1.8 °C), respectively. Average annual precipitation is 865 mm, while the daily mean global radiation shows on average the highest peak in June (526 W m^{-2}) and the lowest in January (143 W m^{-2}; https://surfobs.climate.copernicus.eu/; accessed on 03 March 2022).

The study was conducted in five olive groves (sites 1–5), characterized by different planting ages, density and management practices (Table 1). The soil texture was mainly sandy loam, even if there were some soil differences among the study sites (Table 1; https://www.regione.toscana.it/-/geoscopio; accessed on 03 March 2022).

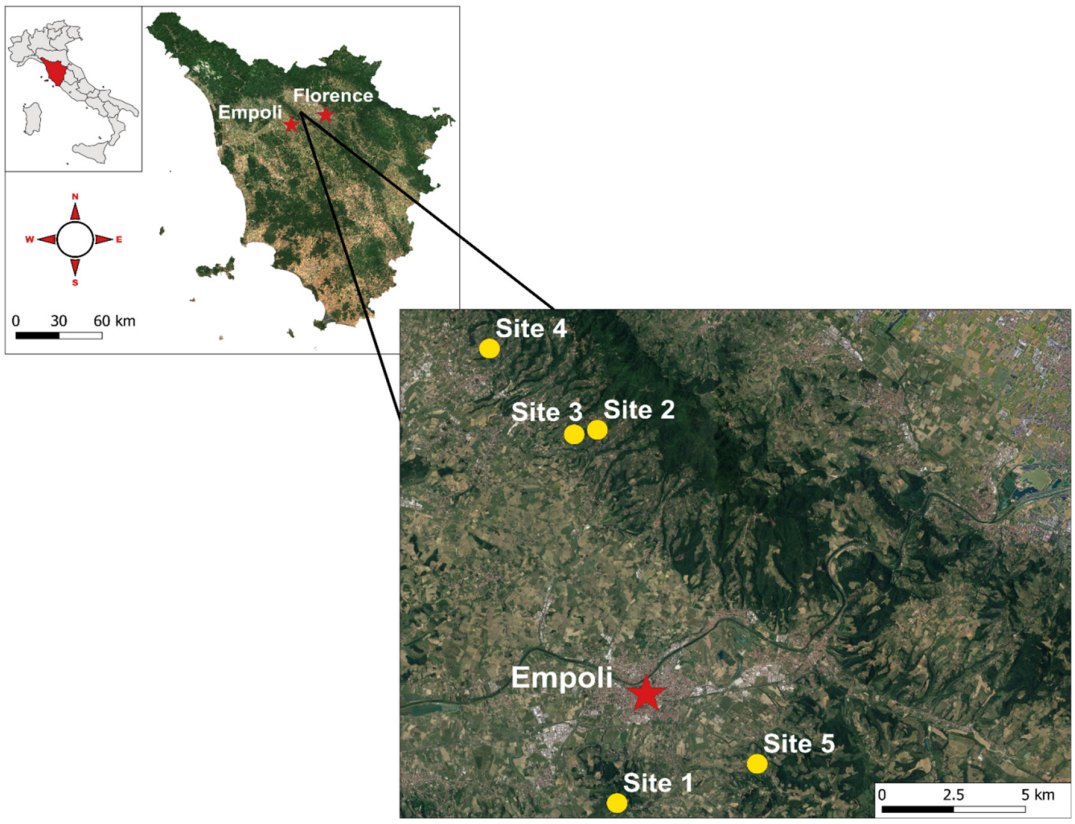

Figure 1. Study area and experimental sites (1–5) in hilly and flat areas of Montalbano district (Tuscany, Italy).

Table 1. Description of the five test sites with relative plant, soil and management characteristics.

	Site information	Site 1	Site 2	Site 3	Site 4	Site 5
Olive trees characteristics and management	*Location*	43.68 °N, 10.93 °E	43.81 °N, 10.93 °E	43.81 °N, 10.92 °E	43.83 °N, 10.88 °E	43.69 °N, 10.99 °E
	Varieties	Frantoio, Moraiolo, Leccino	Frantoio, Moraiolo, Leccino	Frantoio, Leccino, Maurino	Frantoio, Moraiolo, Leccino	Frantoio, Moraiolo, Leccino
	Plant age	>70 y	35–40 y	~25 y	~13 y	~8 y (young plants), ~50 y (old plants)
	Planting density	6 × 11 m	5 × 6 m *	4.5 × 4.5 m *	5 × 6 m *	5 × 6 m
	Training system	Polyconic vase	Polyconic vase	Polyconic vase	Polyconic vase	Polyconic vase
	Pruning period	March–May	March	March–May	February–March	January–February
	Fertilization period	April	March	January + May	March	December–January
	Fertilization type	Organic mixed	Organic mixed	Organic	Organic mixed	Organic mixed
	Pest control period (B. oleae)	July–September	July–September	July–September	July–September	July–September
	Pest control type (B. oleae)	Integrated Pest Manag.	Integrated Pest Manag.	Organic Pest Manag.	Integrated Pest Manag.	Chemical Manag.
	Harvest period	October–December	October–December	October–December	October–December	October–November
	Harvest type	Mechanical (vibrating rakes)	Mechanical (vibrating rakes)	Mechanical (vibrating rakes)	Mechanical (vibrating rakes)	Mechanical (vibrating rakes)
Soil characteristics and management	*Inter-row treatment*	Tillage (June)	Grass cutting (3 cuts/y)	Grass cutting (2 cuts/y), olive pomace, soil milling	Grass cutting (3–4 cuts/y), soil milling after fertilization	Grass cutting (1–2 cuts/y)
	Clay (%)	16	12	12	12	39
	Sand (%)	61	56	56	56	10
	Silt (%)	23	32	32	32	51
	Org. Matter (%)	2.3	1.5	1.5	1.5	1.5

* No regular planting density.

2.2. Field Data Collection and Images Acquisition

The data were collected for the period 2018–2021 in all five study sites. The fPAR was measured over two periods: in June, at phenological stages of fruit-set (BBCH 69); and in September, at olive color change (BBCH 80). In 2021 and only for sites 1 and 5, two additional field campaigns were conducted in order to evaluate the fPAR pattern during dry periods.

The fPAR was measured with an AccuPAR LP-80 Ceptometer (Decagon Devices, Inc., Pullman, Wash), considering the ratio between PAR below (PAR_b) and above (PAR_a) of the olive tree canopies.

$$1-\frac{PAR_b}{PAR_a}$$

All fPAR data were collected each meter along a transect line and below the olive tree canopies. The transect lines covered a total of 43 pixels, and in detail: 17 (two rows of 52 m each), 6 (two rows of 22 m each), 8 (one row of 43 m), 8 (one row of 47 m) and 4 (eight rows of 20 m each) for sites 1 to 5, respectively. Furthermore, planting density, two orthogonal diameters (m) of the canopy crown, and height (m) of olive trees were also measured at each study site.

Sentinel-2 images (2A product-surface reflectance) at a pixel resolution of 10 m were downloaded from the official Copernicus Open Access Hub (https://scihub.copernicus.eu; accessed on 12 January 2022) for each site during the period of the field campaigns (2018–2021). The images (Red Green Blue, RGB, and Near InfraRed, NIR) were post-processed in the R software environment (version 4.1.2) by removing clouds and shadows using the Scene Classification algorithm of the Sentinel-2 toolbox. All seasonal cloud-free images were used for analyzing the VIs trends in each study site while only the cloud-free images close to sampling dates, with a minimum distance of 0 days to a maximum of 9 days with ground observations, were adopted for comparing VIs-derived and observed fPAR.

2.3. VIs Estimation

Five VIs were calculated for each 10 m pixel of Sentinel-2 images in the study sites using the following equations:

(i) Global Environment Monitoring Index (GEMI; [21]):

$$\mathrm{GEMI} = \left(n \cdot (1 - 0.25 \cdot n) - \left(\frac{R - 0.125}{1 - R} \right) \right) \quad (1)$$

$$n = \frac{2 \cdot (NIR^2 - R^2) + 1.5 \cdot NIR + R \cdot 0.5}{NIR + R + 0.5} \quad (1.1)$$

(ii) Modified Chlorophyll Absorption in Reflectance Index 2 (MCARI2; [23]):

$$\mathrm{MCARI2} = 1.5 \cdot \left(\frac{2.5 \cdot (NIR - R) - 1.3 \cdot (NIR - G)}{\sqrt{(2 \cdot NIR + 1)^2 - (6 \cdot NIR - 5 \cdot \sqrt{R}) - 0.5}} \right) \quad (2)$$

(iii) Normalized Difference Vegetation Index (NDVI; [26]):

$$\mathrm{NDVI} = \frac{NIR - R}{NIR + R} \quad (3)$$

(iv) Optimized Soil Adjusted Vegetation Index (OSAVI; [22]):

$$\mathrm{OSAVI} = (1 + Y) \cdot \frac{NIR - R}{NIR + R + Y} \quad (4)$$

With $Y = 0.16$

(v) MCARI2/OSAVI ratio ([22,23]):

$$\mathrm{MCARI2/OSAVI} = \frac{1.5 \cdot \left(\frac{2.5 \cdot (NIR - R) - 1.3 \cdot (NIR - G)}{\sqrt{(2 \cdot NIR + 1)^2 - (6 \cdot NIR - 5 \cdot \sqrt{R}) - 0.5}} \right)}{(1 + Y) \cdot \frac{NIR - R}{NIR + R + Y}} \quad (5)$$

With $Y = 0.16$.

where *NIR* = Near Infra-Red (~ 833 nm), *R* = Red (~ 665 nm) and *G* = Green (~ 560 nm) bands (https://sentinels.copernicus.eu/; accessed on 12 January 2022).

2.4. VIs Rescaling and fPAR Estimation on a Pixel Scale

The initial VIs values (GEMI, MCARI2, NDVI, OSAVI and MCARI2/OSAVI) obtained for the pixels under analysis were partitioned for woody and grass layers by considering the relationship existing between olive tree fraction canopy cover (FC) and the value of relevant VI (Figure 2). Firstly, the olive tree volume coverage was calculated using the measured crown diameters and plant height as a basis to construct an ellipsoid for each of the olive trees present in the Sentinel-2 pixel (Table S1; Figure 2A). Then, olive tree volume, expressed as the percentage of a 3D Sentinel-2 pixel (Figure 2B; Table S2), was correlated to the VIs signal to extrapolate the potential VIs at full olive tree coverage (Figure 2C; Table S3). In this context, the trend of the Pearson's correlation coefficient, slope and intercept values of the VIs-olive tree volume correlations were analyzed during the season, for identifying the highest performing models from which the potential VIs at full olive tree coverage have been extracted. These last potential VIs values were then rescaled with the actual olive tree volume in the pixel to its actual value, following [18,27]. Linear relationships between rescaled VIs and the relevant measured fPAR were then fitted and

validated in areas with contrasting climates and management practices to test the robustness of the proposed strategy. Finally, the previous linear relationships were evaluated during the season by comparing the rescaled VIs with the fPAR field observations mainly collected in June and September. Only for sites 1 and 5 in 2021, the VIs-fPAR correlations were assessed using a more detailed temporal resolution covering almost every month of the vegetation period (April-September; Table S2).

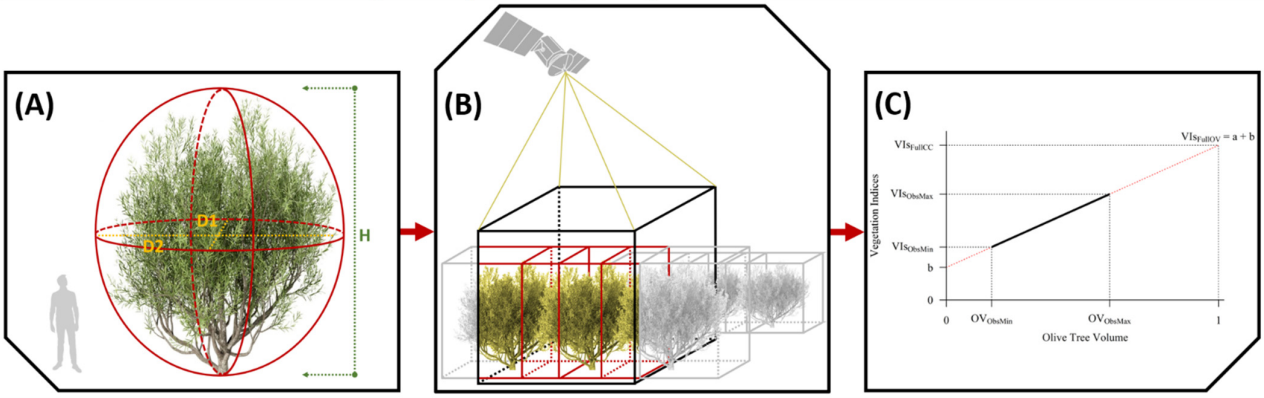

Figure 2. VIs rescaling procedure based on the olive tree volume coverage. (**A**) Ellipsoid shape of the olive tree calculated on the observed diameter and plant height; (**B**) estimation of the olive tree volume coverage in the pixel of Sentinel-2; (**C**) potential Vis' value extraction based on the previous information. VIs$_{ObsMax}$ and VIs$_{ObsMin}$ are the maximum and minimum observed VI values for all pixels of the Sentinel-2 image, respectively. OV$_{ObsMax}$ and OV$_{ObsMin}$ are the maximum and minimum olive tree volume coverage in the Sentinel-2 pixels, respectively. VIs$_{FullCC}$ corresponds to VI at full olive tree coverage.

2.5. Statistical Analysis

The model performances for calibration and validation were assessed using the Pearson's correlation coefficient (*r*, Equation (6)), the Coefficient of Residual Mass (*CRM*, Equation (7)), the Modeling Efficiency coefficient (*EF*, Equation (8)) and the Relative Root Mean Squared Error (*RRMSE*, Equation (9)).

$$r = \frac{\sum_{i=1}^{n}(O_i - \overline{O}) \cdot (P_i - \overline{P})}{\sqrt{\sum_{i=1}^{n}(O_i - \overline{O})^2 \cdot \sum_{i=1}^{n}(P_i - \overline{P})^2}} \quad (6)$$

$$CRM = \frac{\sum_{i=1}^{n} O_i - \sum_{i=1}^{n} P_i}{\sum_{i=1}^{n} O_i} \quad (7)$$

$$EF = 1 - \frac{\sum_{i=1}^{n}(P_i - O_i)^2}{\sum_{i=1}^{n}(O_i - \overline{O})^2} \quad (8)$$

$$RRMSE = \left[\sum_{i=1}^{n} \frac{(P_i - O_i)^2}{n} \right]^{0.5} \cdot \frac{100}{\overline{O}} \quad (9)$$

where O_i is the observed value, $\bar{O}$ is the average of the observed values, P_i is the predicted value and n is the number of observations.

3. Results

The methodology proposed in this study was used for disentangling the fPAR contribution between olive trees and grass cover, by comparing the field observations of the canopy intercepted radiation with the remote sensed-derived VIs in a pixel of Sentinel-2. Initially, we analyzed the trend of observed fPAR collected in different field campaigns during the vegetative season. The four samplings performed in sites 1 and 5 from April to September revealed a low seasonal variability of fPAR where the peak is observed in May-June (fPAR = 0.35 in site 1, the average for all pixels in May; fPAR = 0.22 in site 5, the average for all pixels in June) in correspondence with the phenological stages of flowering and fruit-set (BBCH 65, 69). Afterwards, the fPAR is maintained stable until September (site 1 = 0.34 on average from May to September; site 5 = 0.21 on average from the peak to the end of the season; olive color change stage, BBCH 80; Table S2). This seasonal trend has been accompanied by equally little variation in olive tree volumes over the study period (e.g., ~0.08 m of the radius variation during season 2018–2021 on average for 10 sample plants of site 1, Tables S1 and S2).

As a prerequisite for the application of the proposed methodology, we initially assessed whether there is a relationship between fraction cover and vegetation indices (Figure 3). Detailing the results for sites 1 and 2, used in the calibration stage, all the tested VIs provided a generally high degree of correlation with olive tree FC, ranging from $r = 0.77$ (GEMI, $p < 0.01$) to $r = 0.67$ (MCARI2/OSAVI, $p < 0.01$; Figure 3a). As a result of the rescaling procedure, five fPAR predicting models were calibrated by regressing each VI, rescaled on pixel scale according to its FC, and the relevant observed olive tree fPAR. All VIs showed a high degree of correlation with fPAR, where NDVI provided the highest performances ($r = 0.96$; *CRM* = 0.00; *EF* = 0.93; *RRMSE* = 9.86) and MCARI2/OSAVI the lowest ($r = 0.87$; *CRM* = 0.00; *EF* = 0.87; *RRMSE* = 13.57).

The robustness of these models was tested against independent datasets, which were pooled together (Table S4, Figures 4 and S6–S8). In this context, the GEMI-derived model preserved a high degree of robustness, ($r = 0.89$; *CRM* = 0.11; *EF* = 0.69; *RRMSE* = 21.71) with the MCARI2/OSAVI-derived model yielding similar performances ($r = 0.87$; *CRM* = 0.14; *EF* = 0.58; *RRMSE* = 25.50). Conversely, the model calibrated with MCARI2 resulted in being less robust in simulating fPAR ($r = 0.67$; *CRM* = 0.14; *EF* = 0.12; *RRMSE* = 36.78) with slightly better results for NDVI ($r = 0.78$; *CRM* = 0.10; *EF* = 0.46; *RRMSE* = 28.88) and OSAVI ($r = 0.79$; *CRM* = 0.12; *EF* = 0.44; *RRMSE* = 29.39; Table S4, Figures 4 and S6–S8). This identifies GEMI and MCARI2/OSAVI as the most appropriate indexes for estimating the fPAR of olive tree canopies, regardless of planting densities and soil management practices.

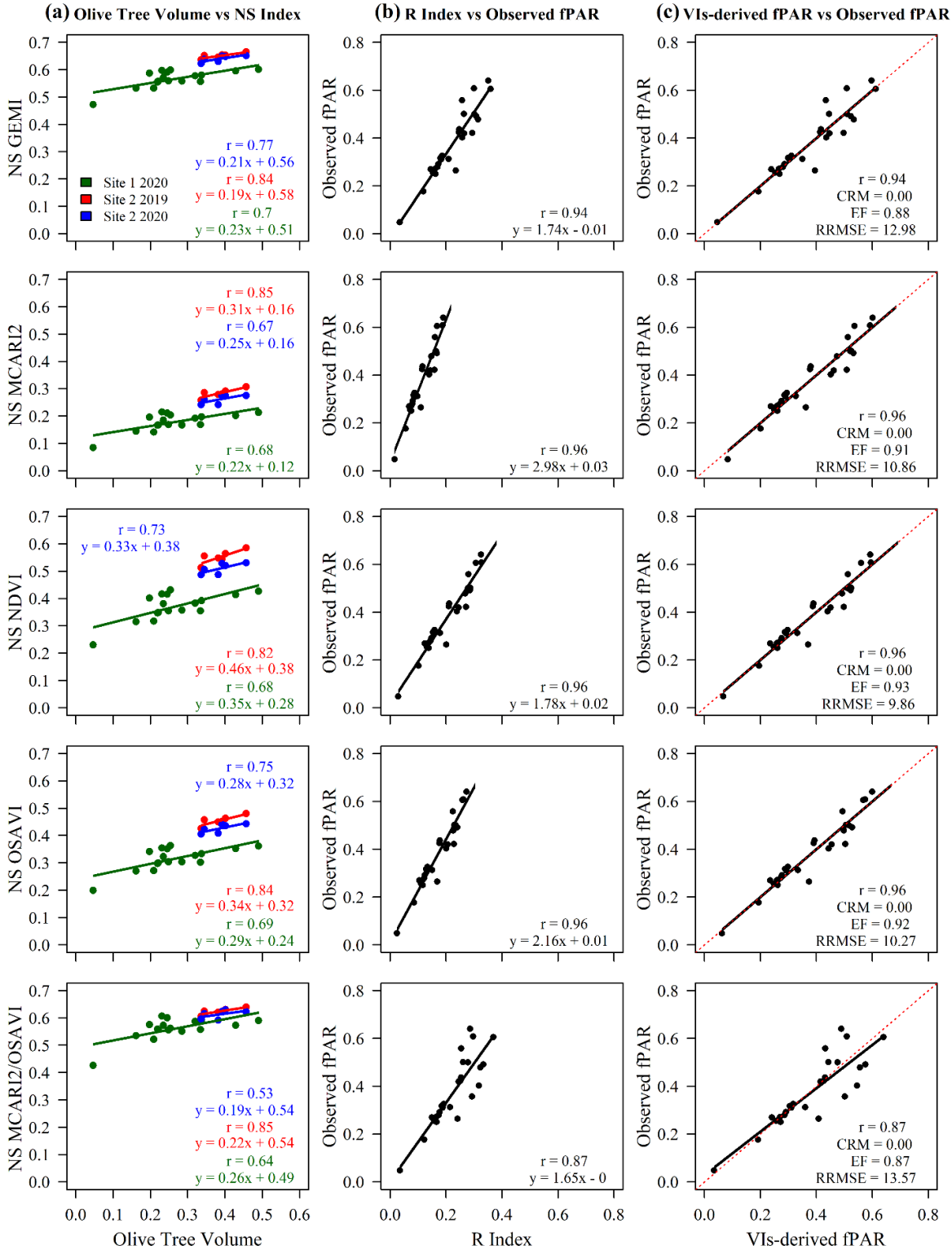

Figure 3. Correlations among the olive tree volume (FC) in the Sentinel-2 pixel and the not re-scaled VIs (**a**); correlations among the rescaled VIs and the fPAR observed in the Sentinel-2 pixel (**b**); correlations among observed and simulated fPAR after calibration (**c**). NS = Not Rescaled; R = Rescaled.

Since these models rely on a VIs–FC relationship obtained for specific dates (e.g., June 2019, 2020 for sites 1 and 2, as shown in Figures 3 and S5), we tested the hypothesis that

the characteristics of the regression line (e.g., intercept, slope and Pearson's correlation coefficient) may vary during the season in response to a different distribution between the herbaceous layer and olive tree canopy (Figure 5 and Figures S1–S4). In site 1 (2018–2021), analyses have demonstrated that the relationship between VIs and FC has a strong seasonal pattern, where the highest slope and Pearson's correlation coefficient and lowest intercept were generally observed in the summer (the driest period). Conversely, in autumn-winter (wet period), the correlation gradually loses its significance (Figures 5 and S1–S4). As a matter of fact, this implies that, for a good partitioning of the signal from remote sensing between herbaceous and tree components, the VIs-FC relationship should be recalibrated during the season in response to different environmental conditions (e.g., wet climate).

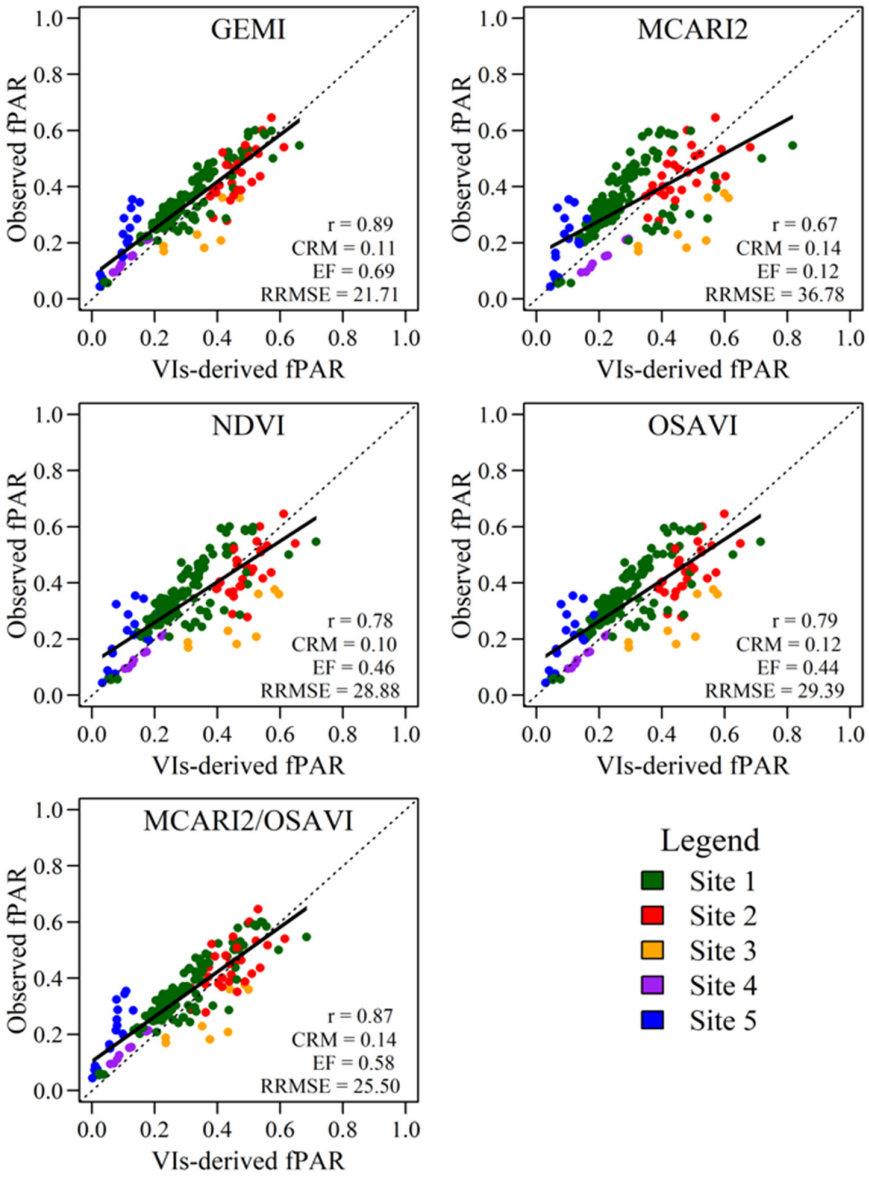

Figure 4. Correlations and statistics between observed and VIs-derived fPAR data obtained for the validation dataset.

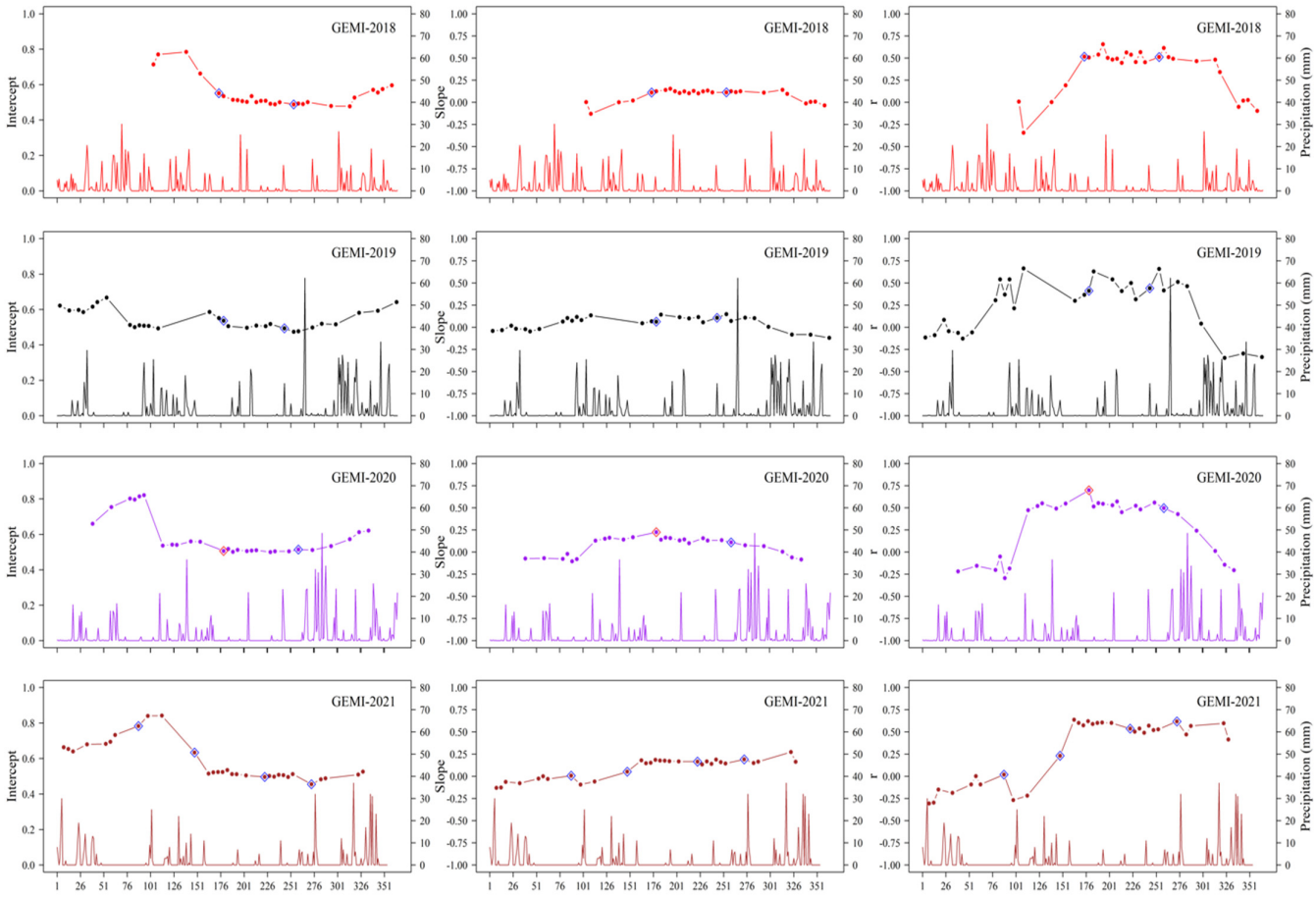

Figure 5. Intercept, Slope and Pearson's correlation coefficient trends derived by the correlation between GEMI and olive tree pixel volume over the period 2018–2021 in Site 1. The seasonal trend of precipitation (mm) for the same period is displayed on the secondary *y*-axis. The data collection dates used for calibration and validation procedure are evidenced by red and blue diamond symbols, respectively.

4. Discussion

This work had two main objectives, the first one consisted of evaluating a methodology to partition the signal from remote sensing and to identify the contribution due to olive trees in areas characterized by different climates, plant density, pruning system and soil management practices. The second goal was to apply the results of this methodology to test the effectiveness of five VIs to provide a robust fit fPAR at pixel scale.

Partitioning the VIs' signal in mixed pixels is a crucial step for improving the estimation of ecosystem processes by using freely available optical satellite imageries [18,27,28]. Although the spatial resolution of most remote sensing platforms could be adequate for crop monitoring growth and production at full canopy cover [29–31], it does not allow the VI contribution to be disentangled between woody and grass layers in olive groves, thus resulting in being less effective in monitoring the actual olive tree growth processes during the season.

The procedure proposed in this work has proved effective in highlighting the different contributions of the woody and herbaceous parts by using the satellite signal of Sentinel-2, paving the way for determining the value of the canopy intercepted radiation relevant to olive trees and grass cover during the season. To achieve this purpose and for evaluating the reliability of rescaled VIs and fPAR correlations, the methodology was cal-

ibrated and validated in typical Mediterranean olive groves characterized by different olive tree canopy dimensions, planting density, climates and management practices, all aspects that unavoidably affect the radiation interception processes [15,32–34].

Initially, the VIs signal was rescaled by considering the volume actually occupied by the foliage of olive trees within a constant volume determined by the size of the pixel of Sentinel-2 (10 × 10 m) and from the maximum height of olive trees assumed to be 5 m. Differently from approaches where signal partitioning relies on the use of crop fraction cover calculated as the orthogonal projection of the canopy on the ground in a 2D space [18,27,28], our approach takes its cue from the fact that olive canopies, even with same projection to the ground, can differ in height, thus significantly altering the relationship between the fraction cover and the VIs (Figure 2). As a consequence, for the same fraction cover, the VIs may greatly change from relatively low (low canopy thickness) to relatively high (high canopy thickness). The 3D rescaling procedure we proposed tried to remove this possible bias resulting in a more accurate methodology for estimating fPAR compared to the two-dimensional approach.

Considering the seasonal dynamics of the components of the olive agroecosystem, we recalibrated the function used for signal partitioning during the season. The analysis of the intercept, slope and Pearson's correlation coefficient of the VIs-olive tree volume relationship for the different VIs demonstrated that the slope of this relationship gradually increases during the season (from winter-spring to summer), leading to a higher VI extrapolated to a fraction cover = 1, as the effect of an increased LAI. At the same time, the intercept, which corresponds to fraction cover = 0 (i.e., grass cover = 1) is higher in spring, when grass is still in full development, and gradually decreases up to summer, when the VIs signal is mostly due to the olive tree canopy only, as in a Mediterranean climate grass development gradually declines in this season, due to summer drought. In autumn-winter, this trend is reversed as increased rainfall results in a progressive re-greening of the grass layer [16], which also offsets the significance of the relationship (Figures S9–S10). This trend suggests that the approach we proposed about the seasonal re-calibration of VIs-FC correlation could be simplified by extracting a single seasonal potential VI value from the olive tree-VIs correlation (Figure S5). Similar to seasonal weather conditions, the trend of the VIs-FC correlation may be affected by agro-management practices during the season. In site 1, for example, the inter-row tillage at the end of May-beginning of June contributes to reducing the intercept value of the VIs-olive tree volume correlation. Compared to grass cutting, the application of tillage, by removing inter-row grass and simulating the previous conditions during dry periods, improved the simulation of the olive tree fPAR from satellite-derived VIs (Figures S9–S10).

Despite the seasonal variability of the VIs-FC relationship, we found that this remains in any case stable for most of the spring-summer (dry period) as evidenced in Figures 5 and S1–S4 for the intercept and slope of the VIs-FC correlation (from June to September). Indeed, considering that the FC of mature olive trees does not change significantly during the vegetative season, as shown in the Results section, our approach can be simplified by using a single olive tree volume-VIs correlation, calibrated at the beginning of the dry period, for rescaling the VI value and simulating fPAR (Figures S5-S8). In this context, the behavior of GEMI and MCARI2/OSAVI, obtained under different sites (1 and 2) and agro-management practices (e.g., tillage vs. grass cutting; Figure 3a) also suggests that some VIs, because of their intrinsic features, can reduce background effects compared to others (e.g., NDVI). This validates our hypothesis of the possibility to adopt a single Vis–olive tree volume correlation at the beginning of the season.

Concerning the VIs behavior, some works indicated NDVI as the most used index for monitoring the biophysical parameters of olive trees [12,35]. However, many applications revealed that this index is less suitable for olive tree monitoring given its high sensitivity to saturation, and atmospheric and soil background effects [19,20,23]. Our results are in line with these observations, as this index proved less robust in simulating the olive tree fPAR in different environmental conditions when compared to the other VIs (Table S4,

Figures 5 and S6–S8). In contrast, GEMI and MCARI2/OSAVI, which were specifically developed for a reduced high sensitivity to saturation and to minimize the atmospheric and soil background effects and the variation to LAI canopy changes [10,21–23], provided a more robust estimation of fPAR, regardless of planting density and inter-row management practices in the validation sites. In this context, the poorest performances were shown by MCARI2, especially when applied to simulate olive tree fPAR (Figure 4).

These poor performances could be due to the rescaled VIs-Observed fPAR correlation during the calibration stage (Figure 3b). Indeed, despite the rescaled MCARI2-Observed fPAR correlation exhibiting higher results (r = 0.96), its high slope value (2.98 vs. 1.74 and 1.65 for GEMI and MCARI2/OSAVI, respectively), determined a higher increase in observed fPAR values to MCARI2 variation. At the same value of rescaled VI, thus, MCARI2 showed higher observed fPAR values compared to the previous VIs, whilst proportionally increasing the value of the rescaled VIs, the increase in observed fPAR determined by MCARI2 was higher than that produced by GEMI and MCARI2/OSAVI (~ 1.71 and 1.81 times higher, respectively). This result was in agreement with [23], which proposed the MCARI2 index as a modified version of the previous MCARI for maximizing the response to green LAI variation. MCARI2, since it is sensitive to NIR reflectance, proved to be a good predictor of the canopy evolution and the variation of vegetation type and structures [36,37]. However, the same sensitivity to NIR variations can make this index variable to the changes in biophysical parameters of canopies, especially under different weather and management conditions (Figures 5 and S9–S10).

Based on the previous considerations, the methodology proposed and the VI-derived fPAR models obtained in this study are able to provide on average an accurate disentangling of the woody and herbaceous fPAR in olive groves. This result may be selected for implementing process-based crop models (e.g., [16]) with the purpose of providing alternative ways to the LAI-based estimates used for the light interception process, by integrating the remotely derived field observations obtained by satellite platform in the model and thus improving the spatial model resolution for seasonal crop monitoring.

5. Conclusions

Satellite imagery is a useful tool for olive tree monitoring and the evaluation of within-field crop variability, providing detailed information for optimizing agro-management practices and farm schedules. However, the spatial resolution of most satellite products does not allow us to accurately estimate the olive groves' dynamics, because of the complexity of a system characterized by two main components: trees and grass.

The methodology proposed in this study demonstrated satisfactory performances when applied to estimate the olive tree fPAR by disentangling the olive tree and grass contribution from five Sentinel-2-derived VIs (GEMI, MCARI2, NDVI and OSAVI, MCARI2/OSAVI) in 10 m pixel resolution. In particular, the olive tree pixel volume-VIs correlation used for rescaling VIs signal provided good performances during the dry period when the grass cover is relatively low by improving the fPAR estimates. In these conditions, the best performances at simulating olive tree fPAR were obtained using GEMI and MCARI2/OSAVI, whilst the poorest performances were reported by MCARI2 likely due to its sensitivity to NIR reflectance variability, which may influence the fPAR overestimation, especially in conditions of high inter-row grass cover. This sensitivity should be considered when remote sensing is used in olive groves, since the two components of this system may be differently influenced by the seasonal weather conditions and management.

In order to address the increasing climatic issues and to approach precision olive growing, the development of a methodology for disentangling olive tree and grass components, as well as the identification of the most adequate VIs for fPAR estimation is essential. Indeed, the approach proposed in this study may allow useful and cost-effective information to be extracted from satellite remote sensing systems, which could be inte-

grated into crop growth models for improving crop monitoring and the evaluation of climate change impacts on agroecosystems. Moreover, this information could also be used to well-schedule agricultural practices, such as pruning, pest and diseases control, irrigation, etc., when coupled to seasonal weather forecasts. In this context, this study paves the way to defining specific strategies for the monitoring of olive groves fPAR, by means of freely available and cost-effective satellite optical products.

Supplementary Materials: The following supporting information can be downloaded at: www.mdpi.com/article/10.3390/agronomy12071540/s1, Table S1: Average olive tree dimensions (diameters and height, m), volume (m3), relative volume and fPAR (observed and observed rescaled) data for all sites and periods (min = mini-mum, max = maximum and avg = average); Table S2: Olive tree volume, fraction cover and observed fPAR in the Sentinel-2 pixel of the experimental sites. Loc = Location; FC = Fraction Cover; "-" = missing data; Table S3: Potential VIs values (GEMI, MCARI2, NDVI, OSAVI, MCARI2/OSAVI) at full olive tree cover in the Sentinel-2 pixel for all combinations of sites and dates. In bold, the VIs values derived from the calibration dataset; Table S4: Results of the correlations between observed and VIs-derived fPAR for each study site and period. The calibration results are in bold; Figure S1: Intercept, Slope and Pearson's correlation coefficient trends derived by the correlation between MCARI2 and Olive tree pixel volume percentage over the period 2018–2021 in Site 1. The seasonal trend of precipitation (mm) for the same period is displayed on the secondary *y*-axis. The data collection dates used for calibration and validation procedure are evidenced by red and blue diamond symbols, respectively; Figure S2: Intercept, Slope and Pearson's correlation coefficient trends derived by the correlation between NDVI and Olive tree pixel volume percentage over the period 2018–2021 in Site 1. The seasonal trend of precipitation (mm) for the same period is displayed on the secondary *y*-axis. The data collection dates used for calibration and validation procedure are evidenced by red and blue diamond symbols, respectively; Figure S3: Intercept, Slope and Pearson's correlation coefficient trends derived by the correlation between OSAVI and Olive tree pixel volume percentage over the period 2018–2021 in Site 1. The seasonal trend of precipitation (mm) for the same period is displayed on the secondary *y*-axis. The data collection dates used for calibration and validation procedure are evidenced by red and blue diamond symbols, respectively; Figure S4: Intercept, Slope and Pearson's correlation coefficient trends derived from the correlation between MCARI2/OSAVI and Olive tree pixel volume percentage over the period 2018–2021 in Site 1. The seasonal trend of precipitation (mm) for the same period is displayed on the secondary *y*-axis. The data collection dates used for calibration and validation procedure are evidenced by red and blue diamond symbols, respectively; Figure S5: Correlations among the olive tree volume and the not re-scaled VIs in the Sentinel-2 pixel. In this case, a single correlation combining different sites and dates was extracted for each VI (a); Correlations among the rescaled VIs and the fPAR observed in the Sentinel-2 pixel (b); Correlations among observed and simulated fPAR after calibration (c). NS = Not Rescaled; R = Rescaled. The correlation among olive tree volume and NS Index was extracted; Figure S6: Comparison between observed and VI-derived fPAR (GEMI, MCARI2, NDVI, OSAVI and MCARI2/OSAVI) over four dates in 2021 and for all pixels of Site 1; Figure S7: Average trend of observed and VIs-derived fPAR (GEMI, MCARI2, NDVI, OSAVI and MCARI2/OSAVI) over four dates in 2021 and for all pixels of Site 1; Figure S8: Average trend of observed and VIs-derived fPAR (GEMI, MCARI2, NDVI, OSAVI and MCARI2/OSAVI) over four dates in 2021 and for all pixels of Site 2; Figure S9: Correlation between observed and VIs-derived fPAR (GEMI and MCARI2) in pixels with different inter-row conditions for four periods (April, May, August and September 2021) in Site 1. The colors of the image legends correspond to the colors of the correlations; Figure S10: Correlation between observed and VIs-derived fPAR (GEMI and MCARI2) in pixels with different inter-row conditions for two periods (July 2021 and September 2020-21) and two sites (Site 2 and 3). The colors of the image legends correspond to the colors of the correlations.

Author Contributions: Conceptualization, L.L., M.M. and S.C.-A.; methodology, M.M., L.L. and S.C.-A.; data curation, S.C.-A., L.L., R.R. and E.B.; formal analysis, L.L., S.C.-A. and M.M.; investigation, L.L., M.M., L.B., Á.L.-B., J.A.S., H.F and C.D. writing—original draft preparation, L.L. and M.M.; writing—review and editing, L.L., M.M., L.B., R.R., J.A.S., H.F., E.B., Á.L.-B., J.A.S., H.F., S.C.-A., C.D. and M.B.; supervision, M.B. and M.M.; project administration, M.B.; funding acquisition, M.B. All authors have read and agreed to the published version of the manuscript.

Funding: This research received funding from OLIVE2REC project "Strategies for marginal olive groves recovering by using new technologies in a context of climate change", Giovani@ RicercaScientifica number 9/2018, funded by Fondazione Cassa di Risparmio di Pistoia e Pescia.

Data Availability Statement: Not applicable.

Acknowledgments: The authors acknowledge the OLIVE2REC project "Strategies for marginal olive groves recovering by using new technologies in a context of climate change", Giovani@ RicercaScientifica number 9/2018, funded by Fondazione Cassa di Risparmio di Pistoia e Pescia and the CATChCO2-live project "The recovery of Tuscany's olive heritage: action to combat climate change for CO2 storage through innovative, cooperative and sustainable land management", PSR-FEASR 2014–2020 Regione Toscana. Finally, all authors acknowledge the farmers and the Montalbano Olio & Vino Soc. Coop. Agr., which gave us the ability to take measurements in the five sites of Montalbano olive groves. This work is also supported by FCT-Portuguese Foundation for Science and Technology, under the project UIDB/04033/2020. H.F. thanks the Portuguese FCT for COA/CAC/0030/2019 and CEEC-IND/00447/2017. The impact of climate change may have a key role in altering the seasonal population dynamics of *B. oleae* (Rossi) and the olive tree phenology by increasing the number of pest generations and severity of this biotic stress.

Conflicts of Interest: The authors declare no conflict of interest.

References

1. ISTAT—Istituto Nazionale di Statistica Coltivazioni: Uva, Vino, Olive, Olio Available online: www.istat.it (accessed on 1 April 2022).
2. Lorite, I.J.; Gabaldón-Leal, C.; Ruiz-Ramos, M.; Belaj, A.; de la Rosa, R.; León, L.; Santos, C. Evaluation of Olive Response and Adaptation Strategies to Climate Change under Semi-Arid Conditions. *Agric. Water Manag.* **2018**, *204*, 247–261. https://doi.org/10.1016/j.agwat.2018.04.008.
3. Brilli, L.; Lugato, E.; Moriondo, M.; Gioli, B.; Toscano, P.; Zaldei, A.; Leolini, L.; Cantini, C.; Caruso, G.; Gucci, R.; et al. Carbon Sequestration Capacity and Productivity Responses of Mediterranean Olive Groves under Future Climates and Management Options. *Mitig. Adapt. Strateg. Glob. Chang.* **2019**, *24*, 467–491. https://doi.org/10.1007/s11027-018-9824-x.
4. Orlandi, F.; Rojo, J.; Picornell, A.; Oteros, J.; Pérez-Badia, R.; Fornaciari, M. Impact of Climate Change on Olive Crop Production in Italy. *Atmosphere* **2020**, *11*, 595. https://doi.org/10.3390/atmos11060595.
5. Moriondo, M.; Bindi, M.; Brilli, L.; Costafreda-Aumedes, S.; Dibari, C.; Leolini, L.; Padovan, G.; Trombi, G.; Karali, A.; Varotsos, K.V.; et al. Assessing Climate Change Impacts on Crops by Adopting a Set of Crop Performance Indicators. *Euro-Mediterr. J. Environ. Integr.* **2021**, *6*, 45. https://doi.org/10.1007/s41207-021-00246-7.
6. Agnoletti, M.; Conti, L.; Frezza, L.; Santoro, A. Territorial Analysis of the Agricultural Terraced Landscapes of Tuscany (Italy): Preliminary Results. *Sustainability* **2015**, *7*, 4564–4581. https://doi.org/10.3390/su7044564.
7. Fraga, H.; Pinto, J.G.; Viola, F.; Santos, J.A. Climate Change Projections for Olive Yields in the Mediterranean Basin. *Int. J. Climatol.* **2020**, *40*, 769–781. https://doi.org/10.1002/joc.6237.
8. Mairech, H.; López-Bernal, Á.; Moriondo, M.; Dibari, C.; Regni, L.; Proietti, P.; Villalobos, F.J.; Testi, L. Is New Olive Farming Sustainable? A Spatial Comparison of Productive and Environmental Performances between Traditional and New Olive Orchards with the Model OliveCan. *Agric. Syst.* **2020**, *181*, 102816. https://doi.org/10.1016/j.agsy.2020.102816.
9. Van Evert, F.K.; Gaitán-Cremaschi, D.; Fountas, S.; Kempenaar, C. Can Precision Agriculture Increase the Profitability and Sustainability of the Production of Potatoes and Olives? *Sustainability* **2017**, *9*, 1863. https://doi.org/10.3390/su9101863.
10. Zarco-Tejada, P.J.; Miller, J.R.; Morales, A.; Berjón, A.; Agüera, J. Hyperspectral Indices and Model Simulation for Chlorophyll Estimation in Open-Canopy Tree Crops. *Remote Sens. Environ.* **2004**, *90*, 463–476. https://doi.org/10.1016/j.rse.2004.01.017.
11. Berni, J.A.J.; Zarco-Tejada, P.J.; Sepulcre-Cantó, G.; Fereres, E.; Villalobos, F. Mapping Canopy Conductance and CWSI in Olive Orchards Using High Resolution Thermal Remote Sensing Imagery. *Remote Sens. Environ.* **2009**, *113*, 2380–2388. https://doi.org/10.1016/j.rse.2009.06.018.
12. Gómez, J.A.; Zarco-Tejada, P.J.; García-Morillo, J.; Gama, J.; Soriano, M.A. Determining Biophysical Parameters for Olive Trees Using CASI-Airborne and QuickBird-Satellite Imagery. *Agron. J.* **2011**, *103*, 644–654. https://doi.org/10.2134/agronj2010.0449.
13. Hornero, A.; Hernández-Clemente, R.; North, P.R.J.; Beck, P.S.A.; Boscia, D.; Navas-Cortes, J.A.; Zarco-Tejada, P.J. Monitoring the Incidence of *Xylella Fastidiosa* Infection in Olive Orchards Using Ground-Based Evaluations, Airborne Imaging Spectroscopy and Sentinel-2 Time Series through 3-D Radiative Transfer Modelling. *Remote Sens. Environ.* **2020**, *236*, 111480.
14. Jorge, J.; Vallbé, M.; Soler, J.A. Detection of Irrigation Inhomogeneities in an Olive Grove Using the NDRE Vegetation Index Obtained from UAV Images. *Eur. J. Remote Sens.* **2019**, *52*, 169–177. https://doi.org/10.1080/22797254.2019.1572459.
15. Caruso, G.; Zarco-Tejada, P.J.; González-Dugo, V.; Moriondo, M.; Tozzini, L.; Palai, G.; Rallo, G.; Hornero, A.; Primicerio, J.; Gucci, R. High-Resolution Imagery Acquired from an Unmanned Platform to Estimate Biophysical and Geometrical Parameters of Olive Trees under Different Irrigation Regimes. *PLoS ONE* **2019**, *14*, e0210804. https://doi.org/10.1371/journal.pone.0210804.
16. Moriondo, M.; Leolini, L.; Brilli, L.; Dibari, C.; Tognetti, R.; Giovannelli, A.; Rapi, B.; Battista, P.; Caruso, G.; Gucci, R.; et al. A Simple Model Simulating Development and Growth of an Olive Grove. *Eur. J. Agron.* **2019**, *105*, 129–145. https://doi.org/10.1016/j.eja.2019.02.002.

17. Spyropoulos, N.V.; Dalezios, N.R.; Kaltsis, I.; Faraslis, I.N. Very High Resolution Satellite-Based Monitoring of Crop (Olive Trees) Evapotranspiration in Precision Agriculture. *Int. J. Sustain. Agric. Manag. Inform.* **2020**, *6*, 43–74. https://doi.org/10.1504/IJSAMI.2020.106539.
18. Maselli, F.; Chiesi, M.; Brilli, L.; Moriondo, M. Simulation of Olive Fruit Yield in Tuscany through the Integration of Remote Sensing and Ground Data. *Ecol. Modell.* **2012**, *244*, 1–12. https://doi.org/10.1016/j.ecolmodel.2012.06.028.
19. Van der Meer, F.; Bakker, W.; Scholte, K.; Skidmore, A.; De Jong, S.; Clevers, J.; Addink, E.; Epema, G. Spatial Scale Variations in Vegetation Indices and Above-Ground Biomass Estimates: Implications for MERIS. *Int. J. Remote Sens.* **2001**, *22*, 3381–3396. https://doi.org/10.1080/01431160152609227.
20. Huang, S.; Tang, L.; Hupy, J.P.; Wang, Y.; Shao, G. A Commentary Review on the Use of Normalized Difference Vegetation Index (NDVI) in the Era of Popular Remote Sensing. *J. For. Res.* **2021**, *32*, 1–6. https://doi.org/10.1007/s11676-020-01155-1.
21. Pinty, B.; Verstraete, M.M. GEMI: A Non-Linear Index to Monitor Global Vegetation from Satellites. *Vegetatio* **1992**, *101*, 15–20. https://doi.org/10.1007/BF00031911.
22. Rondeaux, G.; Steven, M.; Baret, F. Optimization of Soil-Adjusted Vegetation Indices. *Remote Sens. Environ.* **1996**, *55*, 95–107. https://doi.org/10.1016/0034-4257(95)00186-7.
23. Haboudane, D.; Miller, J.R.; Pattey, E.; Zarco-Tejada, P.J.; Strachan, I.B. Hyperspectral Vegetation Indices and Novel Algorithms for Predicting Green LAI of Crop Canopies: Modeling and Validation in the Context of Precision Agriculture. *Remote Sens. Environ.* **2004**, *90*, 337–352. https://doi.org/10.1016/j.rse.2003.12.013.
24. Haboudane, D.; Miller, J.R.; Tremblay, N.; Zarco-Tejada, P.J.; Dextraze, L. Integrated Narrow-Band Vegetation Indices for Prediction of Crop Chlorophyll Content for Application to Precision Agriculture. *Remote Sens. Environ.* **2002**, *81*, 416–426. https://doi.org/10.1016/S0034-4257(02)00018-4.
25. Lima-Cueto, F.J.; Blanco-Sepúlveda, R.; Gómez-Moreno, M.L.; Galacho-Jiménez, F.B. Using Vegetation Indices and a UAV Imaging Platform to Quantify the Density of Vegetation. *Remote Sens.* **2019**, *11*, 2564.
26. Rouse, J.W.; Haas, R.H.; Schell, J.A.; Deering, D.W. Monitoring vegetation systems in the great plains with ERTS. In *Third Earth Resources Technology Satellite-1 Symposium. Volume 1: Technical Presentations, Section A.*; Freden, S.C., Mercanti, E.P., Becker, M.A., Eds.; University of Michigan: Ann Arbor, MI, USA, 1974; Volume 1, pp. 309–317.
27. Maselli, F.; Gilabert, M.A.; Conese, C. Integration of High and Low Resolution NDVI Data for Monitoring Vegetation in Mediterranean Environments. *Remote Sens. Environ.* **1998**, *63*, 208–218. https://doi.org/10.1016/S0034-4257(97)00131-4.
28. Brilli, L.; Chiesi, M.; Maselli, F.; Moriondo, M.; Gioli, B.; Toscano, P.; Zaldei, A.; Bindi, M. Simulation of Olive Grove Gross Primary Production by the Combination of Ground and Multi-Sensor Satellite Data. *Int. J. Appl. Earth Obs. Geoinf.* **2013**, *23*, 29–36. https://doi.org/10.1016/j.jag.2012.11.006.
29. Maselli, F.; Moriondo, M.; Angeli, L.; Fibbi, L.; Bindi, M. Estimation of Wheat Production by the Integration of MODIS and Ground Data. *Int. J. Remote Sens.* **2011**, *32*, 1105–1123. https://doi.org/10.1080/01431160903510799.
30. Ramadhani, F.; Pullanagari, R.; Kereszturi, G.; Procter, J. Mapping of Rice Growth Phases and Bare Land Using Landsat-8 OLI with Machine Learning. *Int. J. Remote Sens.* **2020**, *41*, 8428–8452. https://doi.org/10.1080/01431161.2020.1779378.
31. Xun, L.; Zhang, J.; Yao, F.; Cao, D. Improved Identification of Cotton Cultivated Areas by Applying Instance-Based Transfer Learning on the Time Series of MODIS NDVI. *Catena* **2022**, *213*, 106130. https://doi.org/10.1016/j.catena.2022.106130.
32. Ben Sadok, I.; Moutier, N.; Garcia, G.; Dosba, F.; Grati-Kamoun, N.; Rebai, A.; Khadari, B.; Costes, E. Genetic Determinism of the Vegetative and Reproductive Traits in an F1 Olive Tree Progeny: Evidence of Tree Ontogeny Effect. *Tree Genet. Genomes* **2013**, *9*, 205–221. https://doi.org/10.1007/s11295-012-0548-x.
33. Castillo-Ruiz, F.J.; Castro-Garcia, S.; Blanco-Roldan, G.L.; Sola-Guirado, R.R.; Gil-Ribes, J.A. Olive Crown Porosity Measurement Based on Radiation Transmittance: An Assessment of Pruning Effect. *Sensors* **2016**, *16*, 723. https://doi.org/10.3390/s16050723.
34. Jiménez-Brenes, F.M.; López-Granados, F.; Castro, A.I.; Torres-Sánchez, J.; Serrano, N.; Peña, J.M. Quantifying Pruning Impacts on Olive Tree Architecture and Annual Canopy Growth by Using UAV-Based 3D Modelling. *Plant Methods* **2017**, *13*, 55. https://doi.org/10.1186/s13007-017-0205-3.
35. Solano, F.; Di Fazio, S.; Modica, G. A Methodology Based on GEOBIA and WorldView-3 Imagery to Derive Vegetation Indices at Tree Crown Detail in Olive Orchards. *Int. J. Appl. Earth Obs. Geoinf.* **2019**, *83*, 101912. https://doi.org/10.1016/j.jag.2019.101912.
36. Gu, Z.; Sanchez-Azofeifa, G.A.; Feng, J.; Cao, S. Predictability of Leaf Area Index Using Vegetation Indices from Multiangular CHRIS/PROBA Data over Eastern China. *J. Appl. Remote Sens.* **2015**, *9*, 096085. https://doi.org/10.1117/1.jrs.9.096085.
37. Prada, M.; Cabo, C.; Hernández-Clemente, R.; Hornero, A.; Majada, J.; Martínez-Alonso, C. Assessing Canopy Responses to Thinnings for Sweet Chestnut Coppice with Time-Series Vegetation Indices Derived from Landsat-8 and Sentinel-2 Imagery. *Remote Sens.* **2020**, *12*, 3068. https://doi.org/10.3390/rs12183068.